Author/s:
Turpin, GA;Holt, SA;Scofield, JMP;Teo, BM;Tabor, RF

Title:
Spontaneous Adsorption of Graphene Oxide to Oil–Water and Air–Water Interfaces by Adsorption of Hydrotropes

Date:
2020-05-07

Citation:
Turpin, G. A., Holt, S. A., Scofield, J. M. P., Teo, B. M. & Tabor, R. F. (2020). Spontaneous Adsorption of Graphene Oxide to Oil–Water and Air–Water Interfaces by Adsorption of Hydrotropes. Advanced Materials Interfaces, 7 (9), https://doi.org/10.1002/admi.201901810.

Persistent Link:
https://hdl.handle.net/11343/297984

Spontaneous adsorption of graphene oxide to oil-water and air-water interfaces by adsorption of hydrotropes

Geosmin A. Turpin,[a] Stephen A. Holt,[b] Joel M.P. Scofield,[c]
Boon M. Teo,*[a] and Rico F. Tabor*[a]

[a]School of Chemistry, Monash University, Clayton 3800, Australia

[b]Australian Nuclear Science and Technology Organisation

[c]Polymer Science Group, Department of Chemical and Biomolecular Engineering
The University of Melbourne, Parkville, VIC 3010, Australia

*Corresponding Author E-mail: boonmian.teo@monash.edu, rico.tabor@monash.edu

Keywords: Graphene oxide, Hydrotropes, Adsorption, Emulsification, Foaming, Surface pressure

Abstract

The interfacial adsorption of graphene oxide (GO) is crucial in phenomena such as emulsification and froth flotation, where presence of 2D nanomaterials facilitates Pickering stabilisation. This process usually requires the input of high amounts of shear energy, or is aided by surfactants in order to make it possible at room temperature. In this work, we demonstrate a surfactant-free method for interfacial enrichment through the use of a family of tetraalkylammonium hydrotropes, the most effective being tetraethylammonium chloride (TEAC). As both GO and hydrotropes do not spontaneously enrich to interfaces on their own, this synergistic, spontaneous effect highlights that hydrotropes adsorb to GO sheets, decreasing their nega-

This is the author manuscript accepted for publication and has undergone full peer review but has not been through the copyediting, typesetting, pagination and proofreading process, which may lead to differences between this version and the Version of Record. Please cite this article as doi: 10.1002/admi.201901810

tive charge while rendering them more amphiphilic and therefore making it thermodynamically favourable for them to adsorb to the interface. Evidence for this adsorption includes increases in surface pressure, as well as emulsion and froth stability when both GO and hydrotropes are present in a system. Hydrotropes perform as well as or better than surfactants. Adsorption is irreversible, with XRR and AFM studies demonstrating that roughness increases with compression of the air-water interface, showing that GO sheets are crumpling at the interface rather than desorbing, providing new routes to patterned and structured GO layers.

Introduction

Due to their exceptional physical and chemical properties, two-dimensional (2D) materials show great promise for improving many areas of modern life, from large-scale industrial processes to end-user consumer electronics.[1,2] The advantages of these materials arise from their unique structure, as being atomically thin in one dimension causes them to have unrivalled surface area and unique conductive behaviours.[3,4] Although many other 2D materials have now been discovered, graphene and its derivatives are the most prominently researched[5] due to their superiority in many areas, with graphene being the strongest, thinnest material currently known.[6,7] Another advantage graphene has over other, more "exotic" 2D materials is that the starting materials are allotropes of carbon, such as graphite, which are relatively cheap and abundant.

Although graphene is incredibly promising, it is difficult to synthesise and handle. This motivates an investigation into other 2D materials that share key properties while being easier to handle. One popular target is graphene oxide (GO), produced by applying oxidizing agents and shear to easily exfoliate large amounts of graphite to produce GO with oxygen containing moieties such as carboxyls, phenols and epoxides.[8] Bulk dispersions of GO have two notable advantages over graphene: they are easier to reproducibly synthesise at scale,[9,10] and can be stably dispersed in water due to hydrogen bonding via many oxygen containing groups.[11] These

attributes make GO easier to handle than (hydrophobic) graphene in a range of applications, from pollutant adsorption[12] to aqueous catalysis,[13] with covalent functionalization of GO further expanding these potential applications.[1415]

The combination of a hydrophobic surface with hydrophilic edge groups make GO amphiphilic, conferring an advantage over graphene as it can more easily adsorb to interfaces.[16] This unique structure has provoked great debate whether GO behaves more like a particle or a surfactant at interfaces, with a formative paper published in 2010 by Huang et al. reporting that graphene oxide lowers the interfacial tension of air-water interfaces and therefore acts as a surfactant.[17] In the ten years since this seminal work was published, more recent investigation into this behaviour has demonstrated that this surface activity is actually conferred by oxidative debris present as a byproduct of the exfoliation process, and that extensively purified graphene oxide, free from oxidative debris, is not spontaneously surface active,[18] requiring the presence of a molecular surfactant such as CTAB in order to spontaneously adsorb to the air-water interface.[21]

Being 2D, amphiphilic and exhibiting particle-like behaviour means GO stably adsorbs at interfaces, stabilising oil droplets in water through the formation of Pickering emulsions. Due to the unrivalled surface area of 2D materials, Pickering emulsions stabilised by 2D materials require much less stabiliser than traditional surfactant systems, while forming very stable emulsions.[20] As this process is non-spontaneous at room temperature, it requires the input of energy, usually in the form of shear or sonication.[19] Because surfactants are able to adsorb to GO sheets and spontaneously bring them to interfaces, even at room temperature, these processes can be made less energy intensive through the addition of surfactant, making it possible to stabilise oil-in-water emulsions[21] as well as forming GO foams at the air-water interface with relatively low energetic input.[22] The introduction of stimuli-responsive surfactants adds another dimension of control to these systems, and is an attractive area of further study, an example being light-responsive surfactants causing photoswitchable, reversible aggregation of GO.[23]

Although surfactants work effectively with GO, there are limitations to their industrial application. For example, during crude-oil extraction, surfactants can create emulsions that are too stable, being energetically expensive to eventually demulsify.[24] Another example is surfactants present in paint mixtures causing incomplete coalescence of latex particles, resulting in localised inhomogeneity in dried paints.[25] This motivates the investigation of other amphiphilic molecules that may be able to fulfil a similar role in getting particles such as GO to interfaces, without causing downstream processing problems.

Hydrotrope molecules have been widely applied in industry as they have been shown to synergistically improve bulk solubilisation and stabilisation effects of surfactants,[26] as well as being used as solubilizing agents on their own.[27] The mechanism for hydrotrope action, either in the presence or absence of surfactants, is still contentious, with most discussion focusing on the mechanism of solubilization.[27][28] There has been very little investigation into the behaviour of hydrotropes at interfaces, although they have been shown to increase, for example, the spreading of chlorophyll molecules at interfaces.[29]

Despite not being well understood, wide application in industry of over 46,000 tonnes of hydrotropes per year[30] is a testament to their efficacy and significance, and motivates further investigation. Perhaps because of the difficulty in defining a mechanism of action, it has also proved difficult to determine what exactly classifies as a hydrotrope, as opposed to other, similar amphiphilic solubilizing agents. This is an open area of discussion,[28] with nomenclature often being based simply on the industrial applications of each molecule. For the purposes of this investigation, we start with some molecules definitively classified by previous literature as hydrotropes, before moving into larger analogues of those molecules, some of which have also had their interfacial properties investigated.[27]

There have been some previous investigations into the interactions between particles and some molecules that can be classified as hydrotropes based on application, such as Berol R648,,[31] although the paper more appropriately discusses it in terms of its surfactant-like characteristics. Other investigations into organoclays with smaller molecules definitively defined as hydrotropes, such as tetramethylammonium chloride have been undertaken for industrial contexts such as paper-fining, however their scope of investigation has been system-specific and difficult to translate more widely.[32] This motivates further exploration into the fundamental interactions occurring between hydrotropes and particles with the aim of intelligent control and design of these surfactant-free systems in the future.

1 Results and discussion

1.1 Hydrotropes demonstrate a synergistic surface pressure response with graphene oxide

Pendant drop tensiometry (PDT) measurements show that systems with both GO and hydrotropes present exhibit a surface pressure response (Fig 1a) as the droplet is grown and shrunk in a controlled fashion, indicating that hydrotropes have successfully facilitated GO adsorbing to the interface spontaneously. A surface pressure response upon shrinking a droplet is indicative of the *irreversible* adsorption of particles at the interface, with the GO sheets at the droplet interface buckling upon compression. This crumpling response, rather than having sheets desorbing like a molecular surfactant,[34] is expected when considering how thermodynamically unfavourable it is for GO to desorb from an interface.[35] No surface pressure response is measured in single component negative controls containing either hydrotropes or GO, because neither hydrotropes nor graphene oxide are surface active on their own, requiring the formation of a self-assembled structure to be amphiphilic enough to spontaneously adsorb to the air-water interface. By plotting the relationship between droplet surface area and change in interfacial tension for a given additive, we can gain insight into the mechanism of GO adsorption occurring.

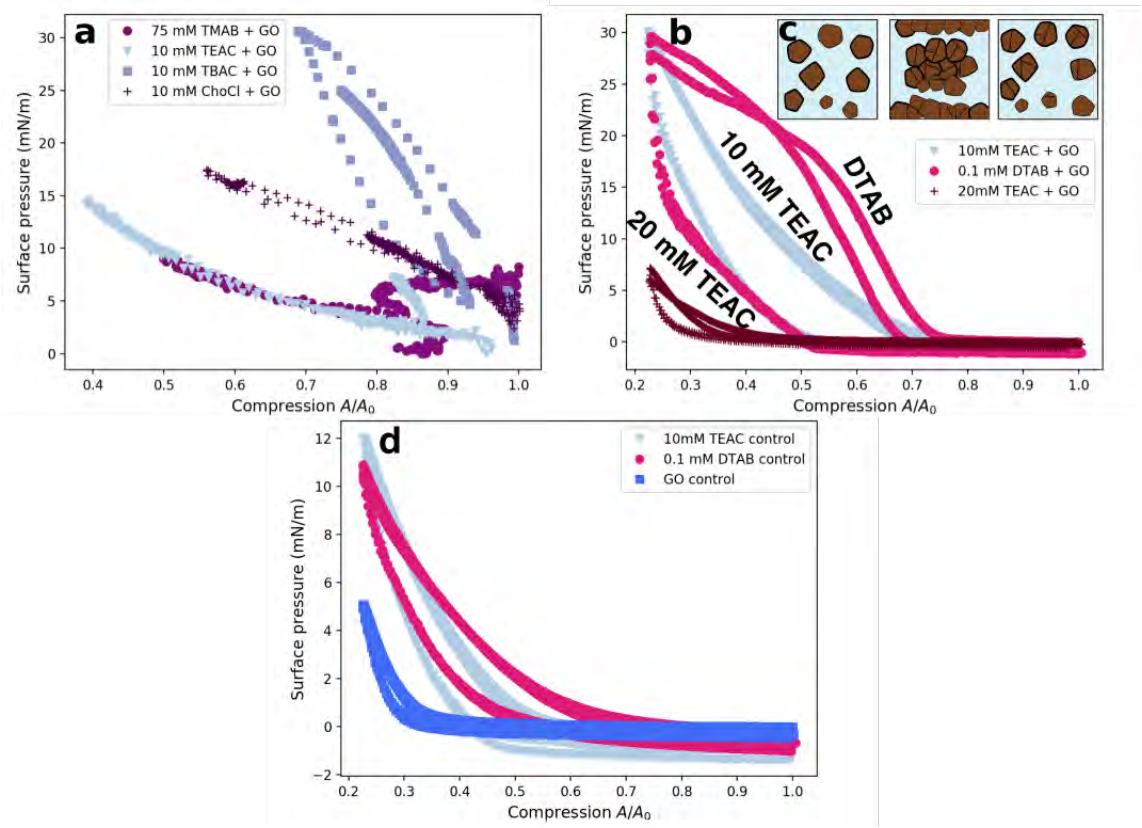

Figure 1: a) Surface pressure plot obtained from pendant drop tensiometry of 0.1 mg/mL aqueous GO dispersions in air with different hydrotropes: tetramethylammonium bromide (TMAB), tetraethylammonium bromide (TEAC), tetrabutylammonium chloride (TBAC), choline chloride (ChoCl). Compression becomes more extreme as data points move from right to left. b) Surface pressure plot obtained from Langmuir trough compression of 0.1 mg/mL aqueous graphene oxide dispersions in air with the hydrotrope tetraethylammonium bromide (TEAC) at two concentrations (10mM and 20mM), as well as a positive surfactant control containing 0.1 mM DTAB. Compression becomes more extreme as data points move from right to left. Inset: c) Schematic diagram showing the three stages of compression of GO sheets at air-water interface. Left: smooth GO sheets before compression. Centre: wrinkled GO sheets during compression. Right: GO sheets remaining wrinkled after relaxation. d) Surface pressure plot obtained from Langmuir trough compression of negative controls in air. Negative controls consist respectively of 0.1 mM DTAB and10 mM TEAC (both without graphene oxide) as well as a negative control containing 0.1 mg/mL aqueous graphene oxide dispersion (with no hydrotrope or surfactant).

There is an apparent hierarchy of surface pressure effects, with the series tetramethylammonium bromide (TMAB)≈ tetraethylammonium bromide (TEAC)< choline chloride (ChoCl)< tetrabutylammonium chloride (TBAC) demonstrating an increased surface pressure response as hydrophobicity of the tetraalkylammonium hydrotropes increases. A steeper gradient corresponds to a greater surface pressure response, indicating that the interface is mechanically stronger and more resistant to deformation, implying that there is more GO at the interface, or that it is adsorbed in a different configuration. TMAB required a higher concentration (75 mM) than TEAC (10 mM) to register a surface pressure response, indicating that increased hydrophobicity through lengthening the alkyl groups still makes TEAC more efficient than TMAB at getting GO to interfaces on a per-molecule basis, potentially linked to Hofmeister effects.[36]

Similar gradients and lack of distinctive hysteresis for the TMAB and TEAC systems indicate that they are likely to facilitate GO adsorption via the same mechanism. Interestingly, ChoCl and TBAC showed different surface pressure responses, with the mild hysteresis of ChoCl indicating some elastic compression as the material crumples, eventually returning to its initial uncompressed state upon relaxation. In contrast to this, the second TBAC compression step registered a greater surface pressure effect than the first step, indicating that some irreversible, plastic compression had occurred, preventing the surface pressure from reaching its previous baseline. As these loops for TBAC appear to have distinct linear regions, this may hint at potential discrete overlaying or crumpling processes at different stages in the compression cycle, and differences in the way hydrotropes and GO are self-assembling at the interface.

The findings from the PDT experiments were verified using a Langmuir trough in order to confirm previous findings and investigate differences in the surface pressure response with better fidelity of data. Graphene oxide with 10 mM TEAC demonstrated a stronger surface pressure response as well as a clearer hysteresis loop than when tested with PDT (Fig 1b-c). This

response was as strong as that of a positive control comprising GO and the surfactant dodecyltrimethylammonium bromide (DTAB), indicating perhaps a similar interfacial enrichment mechanism occurring for GO/hydrotrope systems as what has been previously demonstrated with GO/surfactant systems.[21] Unlike the PDT control measurements, the single component negative control experiments did register a surface pressure response (Fig 1d), but weaker than the GO/trope systems, and only when in compression regimes beyond what is possible to measure using PDT.

The discrepancies between results obtained using PDT and a Langmuir trough may be due to differences in shear when creating and compressing the interface. We would expect modest shear in both systems that we cannot easily quantify, however we would expect the shear of generating a large, rectangular interface in a Langmuir trough to be greater than the low shear required to grow a single droplet. The variation in the area to volume ratio of the systems may also play an effect that warrants further investigation. Interestingly, previous surface pressure measurements with GO and a surfactant demonstrate an eventual plateau, argued to be due to wrinkling and crumpling of GO.[37] This phenomenon was not observed in our work even at maximum possible compression. This may be because previous work was performed with a higher concentration of GO at an enriched surface, whereas our experiments were undertaken on samples with GO and hydrotropes or surfactants adsorbing to the interface from bulk dispersions.

It is interesting to note that 20 mM TEAC demonstrated a significantly weaker surface pressure response in the presence of GO than 10 mM TEAC. Similar behaviour has been previously seen in studies of GO-surfactant self assemblies,[21] and has been ascribed to the surfactants overcharging the GO sheets, resulting in their favourable redispersion in the bulk solvent. As the zeta potential of these GO-hydrotrope systems does not change significantly with TEAC concentration (Supplementary information, Fig S5), this explanation *cannot* be extended to

GO-hydrotrope systems. An alternate hypothesis is that at a 10 mM concentration, TEAC adsorbs to GO sheets, reducing their negative charge and therefore charge repulsion at the (negatively charged) air-water interface, while simultaneously rendering the GO sheets more hydrophobic. This is observed for TEAC but not for simple inorganic salts because of the hydrophobic character of TEAC as an organic salt. When the concentration of TEAC is doubled to 20 mM, the greater ionic strength screens the remaining negative charge on GO particles, allowing them to pack closer together without experiencing electrostatic repulsion, therefore causing a weaker surface pressure response. An alternative hypothesis is that at higher TEAC concentrations, GO 'pre-aggregates' form in the bulk, reducing the effective concentration of GO available to adsorb. These fundamental interfacial measurements therefore provide useful insight, but also demand a more direct investigation into the composition of the air-water interface in these systems.

1.2 Wrinkling graphene oxide at interfaces through compression

X-ray reflectivity (XRR) measurements confirmed that GO adsorbs to the air-water interface. By performing the experiment in a Langmuir trough at varying compressions, we could also infer that that the roughness of the air-water interface increases with compression, indicative of irreversibly adsorbed GO sheets wrinkling when in the presence of 10 mM TEAC (Fig 2a). A single layer model of ≈ 1 nm thickness was able to fit data sets at all levels of compression, with the thickness of the adsorbed sheets being consistent with the thickness of a single graphene oxide sheet, and the only differing variable being the roughness of the interface. This is evidence supporting the idea that GO is irreversibly adsorbing to the air-water interface, with the previously observed surface pressure responses being due to the sheets wrinkling at the interface, rather than desorbing from the interface, or sheets sliding over each other (causing a decrease or increase in the interfacial thickness, respectively). As all reflectivity profiles were baseline corrected by the subtraction of the reflectivity profile of a pure water sample, the $A/A_0 = 0.2$ reflectivity profile dropping into the noise region more dramatically is consistent with it being

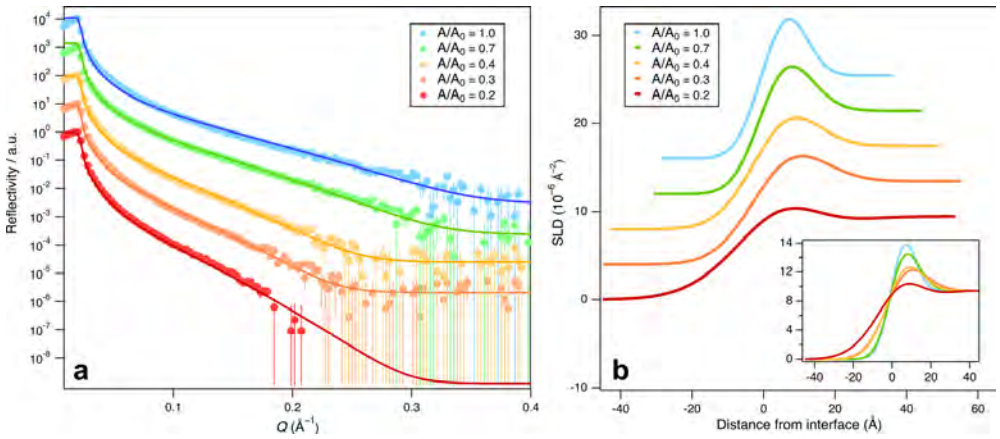

Figure 2: a) X-ray reflectivity data of samples containing 0.1 mg mL^{-1} GO and 10 mM TEAC at the specified compression levels. The filled circles represent the experimental data points and the solid lines are model fits. Data have been offset by multiplication for clarity ($\times$1, 10, 100, 1000 and 10,000). b) The corresponding electron density profiles for the results in (a). Data have been offset by multiplication for clarity ($\times$1, 4, 8, 12 and 16). Inset: superimposed profiles for direct comparison. For all X-ray reflectivity data, level of compression increases from top ($A/A_0 = 1.0$, or no compression) to bottom ($A/A_0 = 0.2$).

the roughest interface and therefore less reflective than the water control.

The SLD profiles are similar to those previously reported for GO/surfactant systems,[18] however due to hydrotropes being significantly smaller than surfactant molecules, they could not be confidently included on a discrete layer when fitting the single-layer model. The decrease in SLD as compression occurs is due to the interfacial roughness increasing (Fig 2b), with the smooth, uncompressed interface showing a distinct SLD difference between the GO sheets at 10 Å from the interface and water beyond 30 Å. This then becomes less distinct as the interface becomes more rough, with therefore more contribution from water, until there is difficulty resolving the two. A table containing all MOTOFIT fitting parameters is provided (Supplementary Information, Table S2).

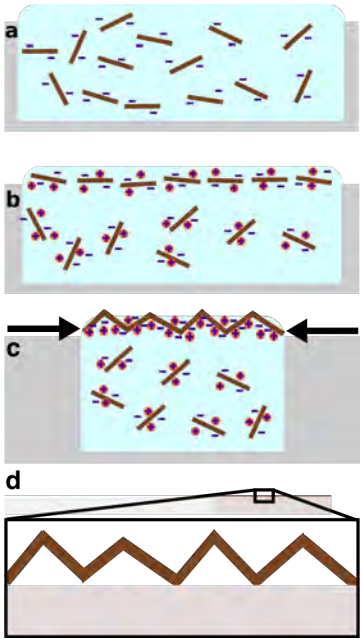

Figure 3: Schematic diagrams of a) GO sheets stably dispersed in water due to strong negative surface charge. b) GO-hydrotrope self assemblies spontaneously adsorbing to the air-water interface after positively charged hydrotropes adsorb to negatively charged graphene oxide sheets. c) Interfacially enriched GO-hydrotrope self assemblies wrinkle upon compression of the interface. d) Wrinkled GO is successfully transferred to glass slide after dip-coating and is ready to be measured via AFM.

Although X-ray reflectivity is useful for assessing roughness and interfacial thicknesses, it is difficult to ascertain complex topographical information with it due to the large area from which signal is averaged. We therefore used atomic force microscopy (AFM) in order to gain a more direct local image of what was occurring during the compression process. This was achieved by dip coating a glass slide through the interface of a mixture of GO and 10 mM TEAC at different levels of compression and allowing slides to dry, with a schematic being provided in order to visualise the proposed mechanism (Fig 3). When these samples were imaged using AFM, this experiment directly demonstrated that (initially flat) GO sheets transferred from the interface to the glass slide become more wrinkled as the interface becomes more compressed during transference (Figs 4a-c), with the wrinkles both becoming taller and increasing in prevalence showing corresponding to GO sheets assembled at the air-water interface being more wrinkled with increasing compression.

Obtaining line profiles (Fig 4d) and measuring roughness allowed us to quantify the increases in roughness and correlate with the trends found via XRR (Fig 4e). Because of differences between the two systems, the absolute values obtained through measuring roughness are not directly comparable, as the AFM measurements were performed on a system with all the roughness constrained to one interface, whereas during XRR the crumpling occurs on both sides of the film, as well as roughness of the film being averaged over a much larger area. Despite this, both measurements demonstrate the same relative trend of GO roughness at the interface increasing as the interface becomes more compressed, indicating that GO is irreversibly adsorbed at the interface and does not desorb upon compression. This does not occur to any significant degree when a negative GO control was measured using XRR or AFM, highlighting the importance of TEAC in order to synergistically drive this process.

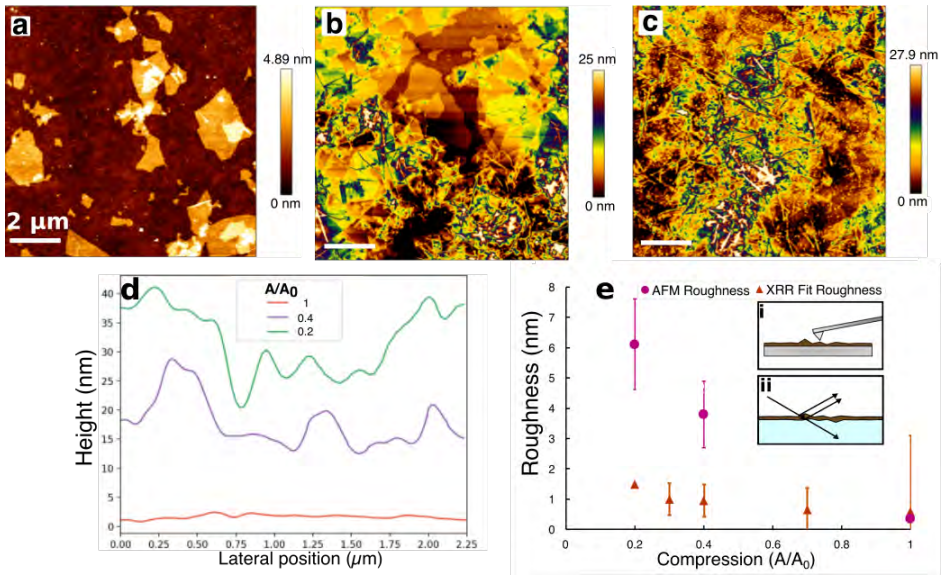

Figure 4: Atomic force microscopy images of graphene oxide dip-coated onto glass slides in the presence of 10 mM TEAC. Images were taken at compression lengths of (a) $A/A_0 = 1$ (uncompressed), (b) $A/A_0 = 0.4$, (c) $A/A_0 = 0.2$ (most compressed). Representative line profiles of each image are shown in (d), with a vertical offset applied for ease of comparison. e) Comparison of roughness at the air-water interface of systems comprising 0.1 mg/mL GO and 10mM TEAC as the interface is compressed, as determined via XRR and AFM. Error bars given for AFM dataset are equal to the standard deviation of the data, error bars for the XRR are equal to the standard deviation of the fit as described in the Motofit package.[39] Error bar is omitted for the most compressed XRR datapoint as the measurement drops below signal-noise ratio at a Q value greater than 0.2 $Å^{-2}$ Inset: schematic diagram demonstrating differences in roughness between dip-coated GO at the i) air-solid interface measured using AFM and GO at the ii) air-water interface measured using XRR.

A similar phenomenon has been seen in a previous investigation using the surfactant CTAB[37] where GO on its own does not increase in surface roughness after being compressed, but GO/CTAB together do. Interestingly, compressing GO on its own still demonstrated a surface pressure effect, albeit with a lower surface compressional modulus, which is posited to be due to GO sheets stacking over each other, whereas the pronounced surface pressure effect and increase in roughness in the GO/CTAB case was due to wrinkling of the surface. This mechanism was argued to be due to CTAB molecules increasing the in-plane rigidity of the GO films, transitioning from sinusoidal wrinkles to S-folds.[40] This previous experiment was performed using an enriched monolayer on the surface, whereas ours is demonstrative of GO adsorbing to the interface from the bulk, however this comparison is still instructive.

1.3 Using graphene oxide and hydrotropes to stabilise interfaces

As hydrotropes can facilitate the spontaneous adsorption of GO to interfaces, an attractive application to explore is stabilising air-water and oil-water interfaces via Pickering stabilisation of emulsion droplets and foams. Because it was characterised via AFM and XRR, TEAC has been selected as a representative hydrotrope for this study, with GO stabilised o/w emulsions in the presence of 10 mM TEAC demonstrating superior long-term stability over a month when compared to emulsions stabilised with pure graphene oxide. Surprisingly, these emulsions were shown to be as, if not more stable than their counterparts stabilised with the surfactant DTAB, motivating further investigation into the application of hydrotropes to improve Pickering emulsification. The stability of other hydrotropes over 96 hours were also examined using microscopy, demonstrating similar increases in stability but slightly larger sizes and polydispersity (Supplementary information, Fig S6).

In the absence of GO, TBAC was the only hydrotrope to facilitate emulsification, and these emulsions coalesced within 6 hours, showing that even if TBAC demonstrates a slight surface ac-

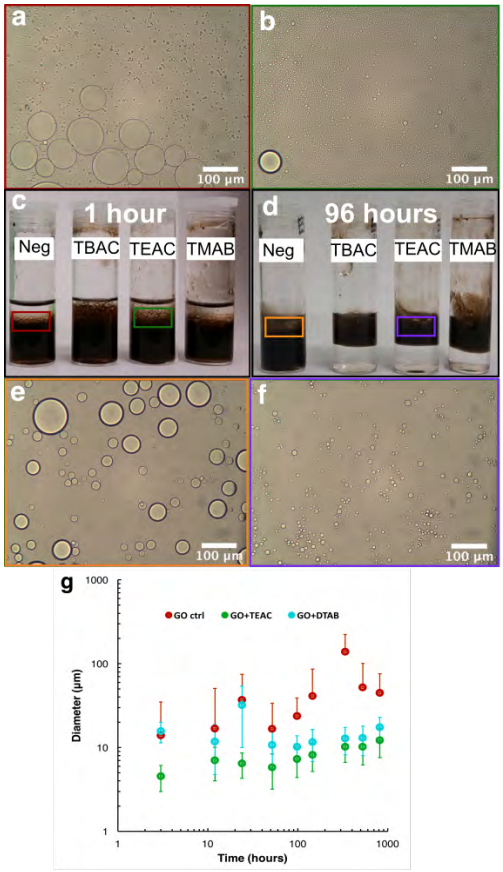

Figure 5: a) n-hexane in water emulsions (1mL n-hexane: 2 mL aqueous dispersion of 1 mg/mL GO), 1 hour after ultrasonic emulsification (10% amplitude for 1 minute followed by 20% amplitude for 1 minute, total power input 1.16 W/mL). Left to right: negative control with GO and no hydrotrope, 10mM TBAC, 10 mM TEAC, 0.1 mM TBAC, 75 mM TMAB. b) Optical light microscopy image of negative control, 1 hour after emulsification. c) Optical light microscopy image of sample with 10 mM TBAC, 1 hour after emulsification. d) Same n-hexane in water emulsions, 1 mg/mL GO, 96 hours after emulsification. e) Optical light microscopy image of negative control, 96 hours after emulsification. f) Optical light microscopy image of sample with 10 mM TBAC, 96 hours after emulsification. g) Scatter plot assessing long term stability of n-hexane in water emulsions, stabilised either with 1 mg/mL GO alone, or with either 10 mM TEAC or 0.1 mM DTAB added. Diameter of droplets was assessed through optical microscopy and averaged with a sample size n=100-200. Error bars correspond to the standard deviation. Negative error bars were omitted from GO control for visual clarity.

tivity, it is GO adsorbing to the interface that confers stability to these systems. This highlights that enhanced Pickering stabilisation was occurring,[18] demonstrating that hydrotropes can also facilitate interfacial enrichment of GO at the oil-water interface. This could occur through two mechanisms, either with hydrotropes decreasing the surface energy of GO at the interface, or making droplets more stable. For a given energy input, stability relies on getting the stabilizer, in this case GO, to the interface quickly enough that negligible coalescence can occur.

The oil-water interfacial tensions of these systems were measured using pendant drop tensiometry, (Supplementary information, Fig S8), with the presence of GO or TEAC slightly lowering interfacial tension, and the presence of both of them synergistically lowering the interfacial tension further. This evidence suggests that the TEAC/GO self assemblies are subtly surface active at oil-water interfaces, contributing further to Pickering stabilisation, while still being possible that this facilitates faster interfacial adsorption.

Another desirable application of Pickering stabilisation is to extract 2D nanomaterials from water through the formation of a foam on top of the aqueous phase, and this work shows that this is possible through the use of hydrotropes. The surfactant CTAB has been previously used to extract GO from water,[22] and so was used as a positive control. The hydrotrope TBAC demonstrated frothing (Fig 6b), while interestingly, unlike the emulsion experiment, the other hydrotropes did not. This is consistent with TBAC demonstrating the strongest response during surface pressure measurements (Fig 1), a further indication that increasing the hydrophobicity of hydrotropes either causes more GO to adsorb to the interface, or causes it to enrich on a shorter timescale. The hydrotrope formed a finer foam than the surfactant control, and over 96 hours, more graphene oxide remained stably at the air-water interface for the CTAB/GO sample, whereas in the TBAC/GO sample, the majority of GO settled over that time.

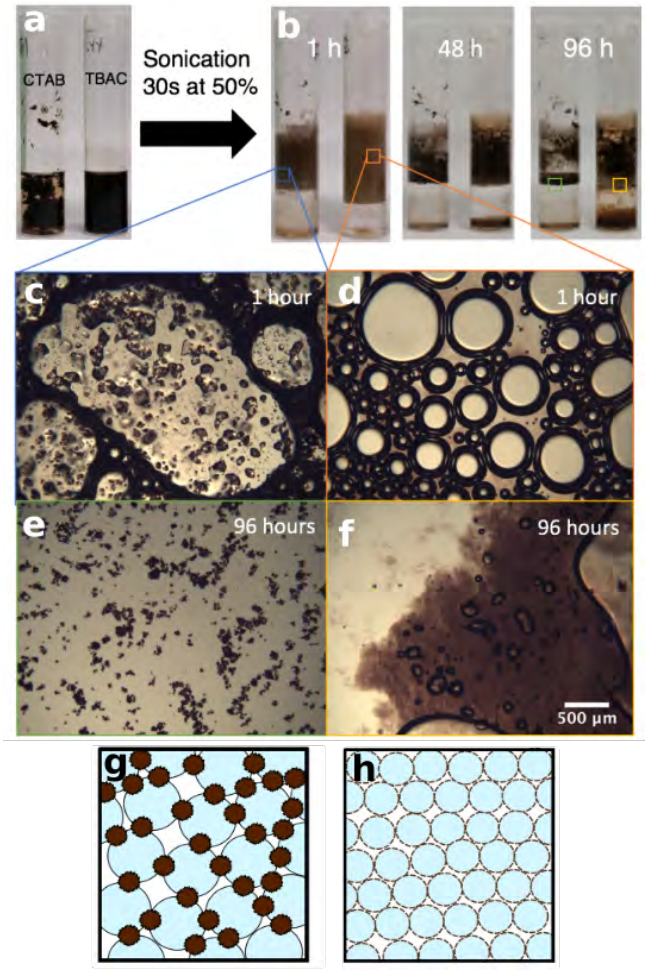

Figure 6: a) 1 mg/mL GO with either positive control (2 mM CTAB), or 10 mM TBAC (right), prior to sonication. b) Same samples either 1, 48, or 96 hours after frothing via interfacial sonication (50% amplitude for 30 seconds, total power input 4.96W/mL). Optical microscopy showing bubbles of c) CTAB/GO system after 1 hour, d) TBAC/GO system after 1 hour, e) CTAB/GO system after 96 hours, f) TBAC/GO system after 96 hours. Schematic diagrams demonstrating g) larger bubbles stabilised by GO aggregates in systems with surfactant present, h) smaller bubbles of a Pickering emulsion formed when hydrotropes facilitate GO spontaneously adsorbing to the air-water interface.

Optical microscopy of bubble structure provided insight into this process. The images reveal CTAB/GO foam bubbles to be highly irregular in shape with GO aggregates entrained in the plateau borders (liquid films) (Fig 6c), indicating that the GO sheets are rendered strongly hydrophobic and are thereby aggregating. This is supported by the CTAB/GO system visibly coagulating prior to sonication (Fig 6a). In contrast to this, the TBAC/GO foam showed spherical, albeit polydisperse bubbles (Fig 6d), indicating the formation of a Pickering foam stabilised by nanoscale anisotropic GO sheets rather than microscale, fractal GO aggregates.[41] These true Pickering foams facilitated by hydrotropes are smaller and finer than the coarse microscale GO aggregates formed by surfactants, explaining the greater foam volume (Fig 6g-h).

This diminished long-term stability of the TBAC/GO sample could be considered an advantage for the hydrotrope system, as it mimics the industrial process of froth flotation: a highly foaming, metastable system allows for material to be extracted, but then re-captured as an easy-to handle, low volume aqueous dispersion rather than a high volume foam that is challenging to break and process. Both foams dried and collapsed after 96 hours, with CTAB/GO aggregating into discrete fractal patterns, whereas TBAC/GO aggregated with less definition, potentially with some bubbles still associated with the aggregate (Fig 6e-f). An important counterpoint to this experiment are the negative controls- without GO, TBAC does still show froth formation, demonstrating some minor interfacial activity, however the foams produced collapse in minutes, confirming the role of GO as a Pickering stabiliser. Without a surfactant or hydrotrope, GO shows no frothing, indicating that energetic input is not sufficient to drive GO to adsorb to the interface, confirming the role of the hydrotrope present to confer spontaneity to the process.

2 Conclusions

This work has demonstrated an effective way to spontaneously adsorb GO to air-water and oil-water interfaces without surfactants, showing Pickering stabilisation of emulsions and foams. This occurs when hydrotropes and GO work synergistically, as neither component is surface ac-

tive on their own. This mechanism is likely to involve positively charged hydrotropes adsorbing to negatively charged GO sheets via charge interactions, rendering their faces more hydrophobic and causing them to be amphiphilic enough to become surface active self-assemblies. Further support for Pickering stabilisation occurring is that this process was shown to be irreversible, as compressing the air-water interface was seen to increase roughness, indicating that the sheets are wrinkling, rather than desorbing like a molecular surfactant. It is especially compelling that the same interfacial model can fit X-ray reflectivity data at all levels of compression, with all variables besides roughness being fixed, and AFM data provided a useful corroboration. These tantalizing findings motivate further exploration into the interactions and applications of hydrotropes with 2D nanomaterials, and more generally with particles at interfaces.

Although this work demonstrates some of the differences between chain length as hydrotrope alkyl-chain length is increased, there is space for further systematic interrogation, as well as examining in more detail the differences between choline chloride and the symmetrical tetraalkylammonium bromide hydrotropes. Given the minimal amount of 2D nanomaterial required to stabilise these systems, with hydrotropes being less toxic, and less difficult to remove from solution than surfactants, this also motivates further investigation into applying these systems as stabilisers. Initial findings show hydrotrope and GO systems to be as or more effective at stabilising emulsions as compared to their surfactant and GO counterpart systems, demonstrating a good shelf-life with little aggregation over a month. Also of interest is the application of hydrotropes as temporary frothing agents allowing for enrichment, removal, and subsequent re-settling of 2D nanomaterials, requiring less processing and purification than their surfactant counterparts. Combining both fundamental and applied investigations of these systems will give the best possible insight into how to apply them, with more understanding of the interactions between GO and hydrotropes hopefully allowing for more intelligent hydrotrope selection and system design in the future.

3 Materials and methods

3.1 Materials

Graphene oxide was synthesised from graphite (Sigma, +100 mesh) using the modified Hummers' method[8] with the additional processing step of being dialysed for 2 weeks in ultra pure water, using cellulose dialysis tubing (Sigma), with water being changed twice daily. Characterization of these materials was performed previously and can be found in the Supporting Information of McCoy et al.[23] As the properties and thus physical behavior of GO and can differ markedly depending on their preparation routes, all samples were made using materials from the same synthesis batch. All hydrotropes (ChoCl, TMAB, TMAC, TEAC, TBAC) and surfactants (DTAB, CTAB) were purchased from Sigma and used without further purification, as was the n-hexane (>99.0%) used for the emulsification experiment.

3.2 Critical coagulation concentration

Batch samples were made up with 0.1 mg/mL GO dispersions and increasing amounts of hydrotropes. Samples were vortexed for 10 seconds before being allowed to settle, with the hydrotropes being added last in order to minimise the effects on any localized concentration gradients. Coagulation was then assessed through visual inspection 2, 12 and 24 hours after preparation.

3.3 Surface pressure measurements

Surface pressure measurements were performed inside a glass cuvette sealed with polytetrafluoroethylene tape. Samples contained 0.1 mg/mL GO dispersions and varying amounts of aqueous hydrotrope, and were dispensed via blunt 1.27 mm needle. Measurements were performed using Opendrop 1.1 open source software[33] with a Flea3 CMOS camera (Point Grey, Richmond, Canada) camera and a home-made pendant drop setup attached to an Adelab syringe pump. Typically, measurements were taken for 4000 seconds, with a droplet having an initial volume

around 14 μL, before being shrunk to approximately 6 μL at around 1000 seconds for 500 seconds, before being left to equilibrate for 500 seconds. After equilibration of the shrunken droplet, it is then grown again at around 2500 seconds for a further 500 seconds until it approximates its original volume, before being left to equilibrate once more to complete the measurement.

3.4 Pendant drop tensiometry measurements

Pendant drop tensiometry measurements were performed inside a glass cuvette sealed with polytetrafluoroethylene tape. Samples contained 0.1 mg/mL GO dispersions and varying amounts of aqueous hydrotrope, and were dispensed via blunt 1.27 mm needle. The continuous phase was n-hexane. Measurements were performed using Opendrop 1.1 open source software[33] with a Flea3 CMOS camera (Point Grey, Richmond, Canada) camera and a home-made pendant drop setup attached to an Adelab syringe pump. Measurements were taken until the interfacial tension reached a plateau.

3.5 Zeta potential

Zeta potential measurements were performed on 0.1 mg/mL dispersions of GO using phase analysis light scattering (PALS) on a Brookhaven Nanobrook Omni instrument. Each measurement involved 5 consecutive runs comprising 20 cycles at 25 °C.

3.6 X-ray reflectivity

XRR measurements of the air-water interface were performed using a PANanalytical X-Pert PRO reflectometer (high tension = 45 kV, current = 40 mA) with a radiation wavelength (Cu K_α) of 0.15418 nm. Measurements were 60 min in duration, during which the incident angle was increased from ≈0.01 to 0.99 Å^{-1} (Q range). The specular reflectivity was thus observed as a function of the momentum transfer perpendicular to the sample surface. Samples were contained in a teflon Langmuir trough (7 cm × 15 cm × 0.4 cm) and sealed in a closed environment to minimize evaporation. The reflectometer enclosure temperature was ≈26°C. All reflectivity

data was modelled using MOTOFIT,[39] a reflectivity analysis software package run from the IGOR Pro environment. Further details regarding modelling can be found in the Supporting Information.

3.7 Dip coating

Dip coating was performed on plasma cleaned glass slides cut into 3cm pieces. The coating dispersion was 500 mL of 0.1 mg/mL GO with and without 10 mM TEAC, in a teflon Langmuir-Blodgett trough (76 cm $\times$ 10 cm, Nima Technology Ltd.). Surface pressure was measured using a Wilhelmy plate (2.35 cm $\times$ 1 cm, Whatman CHR1 filter paper) attached to a pressure sensor. Surface pressure-area isotherms for these systems were performed at a rate of 36 mm/min. Coating was performed with the substrate initially submerged, and retracted from the dispersion medium at a rate of 3 mm/min. Coating was performed in one pass, on different slides each time, at 3 different compression points- uncompressed, at 40% of the original area, and at 20% of the original area, with the interface being compressed and held at the target area during the coating process. Slides were allowed to air-dry before being stored at room temperature in a plastic petri dish.

3.8 Atomic force microscopy

Height profiles of dip-coated glass were taken using a JPK Nanowizard 3 in AC (Alternating contact mode) in air, with Bruker Model NHCV cantilevers, with nominal resonant frequencies of 340 kHz.

3.9 Emulsification experiment

Samples comprised an oil phase containing 1 mL of n-hexane, and 2 mL of an aqueous phase containing 1 mg/mL GO and either 10 mM tetrabutylammonium chloride, 10 mM tetraethylammonium chloride, 0.1 mM tetrabutylammonium chloride or 75 mM tetramethylammonium bromide. Negative controls were run containing GO with no hydrotrope, and hydrotropes with

no GO. Emulsification was achieved through ultrasonic dispersion using a Branson digital sonifier, (400 W) at 10% amplitude for 1 minute followed by 20% amplitude for 1 minute (total power input 1.16 W/mL) with the tip positioned at the boundary between oil and water phases. Macroscopic stability was assessed visually at 1, 48, and 96 hours. Microscopic structure of droplets was assessed via optical light microscopy using a CMOS camera (Flea3, Point Grey, Richmond, BC, Canada) connected to a Kozo XJP-300 polarising microscope with the polarising filters removed. Measurements were taken multiple times per day for the first 3 days, and then repeated once every 2-3 days for a month to assess long term stability.

3.10 Froth flotation experiment

Samples comprised aqueous 1 mg/mL GO dispersions with either 10 mM tetrabutylammonium chloride, 10 mM tetraethylammonium chloride, or 75 mM tetramethylammonium bromide, as well as a positive control containing 2 mM CTAB surfactant instead of hydrotrope, and a negative control containing 75 mM NaCl instead of hydrotrope. Macroscopic stability was assessed visually at 1, 48, and 96 hours. Foams were formed via ultrasound using a Branson digital sonifier, (400 W) at 50% amplitude for 30 seconds (total power input 4.96W/mL). Tip was carefully placed directly at air-water interface, as no frothing occurs if the tip is too deeply submerged. Microscopic structure of foam was assessed via optical light microscopy using a CMOS camera (Flea3, Point Grey, Richmond, BC, Canada) connected to a Kozo XJP-300 polarising microscope with the polarizing filters removed.

Conflicts of interest

The authors declare there are no conflicts of interest.

Acknowledgements

The authors would like to acknowledge the Australian Centre for Neutron Scattering, Australian Nuclear Science and Technology Organisation, for use of their X-ray reflectivity instrumentation (P7477). This work was supported in part by the grant of an ARC Future Fellowship (FT160100191) to R.F.T. and both an Australian Government Research Training Program Scholarship and a Monash Graduate Excellence Scholarship to G.A.T.

References

[1] Y. Zhu, S. Murali, W. Cai, X. Li, J. W. Suk, J. R. Potts, R. S. Ruoff. *Adv. Mater.* **2010**, *22*, 35 3906.

[2] K. Zhang, X. Yang, D. Li. *J. Energy Chem.* **2018**, *27*, 1 1.

[3] Y. Zhang, Y.-W. Tan, H. L. Stormer, P. Kim. *Nature* **2005**, *438*, 7065 201.

[4] P. Montes-Navajas, N. G. Asenjo, R. Santamaría, R. Menéndez, A. Corma, H. García. *Langmuir* **2013**, *29*, 44 13443.

[5] E. P. Randviir, D. A. Brownson, C. E. Banks. *Mater. Today* **2014**, *17*, 9 426 .

[6] C. Lee, X. Wei, J. W. Kysar, J. Hone. *Science* **2008**, *321*, 5887 385.

[7] A. K. Geim. *Science* **2009**, *324*, 5934 1530.

[8] D. C. Marcano, D. V. Kosynkin, J. M. Berlin, A. Sinitskii, Z. Sun, A. Slesarev, L. B. Alemany, W. Lu, J. M. Tour. *ACS Nano* **2010**, *4* 4806.

[9] B. R. Coleman, T. Knight, V. Gies, Z. J. Jakubek, S. Zou. *ACS Appl. Mater. Interfaces* **2017**, *9*, 34 28911.

[10] A. A. Green, M. C. Hersam. *J. Phys. Chem. Lett.* **2010**, *1*, 2 544.

[11] Y. Jiang, R. Raliya, J. D. Fortner, P. Biswas. *Environ. Sci. Tech.* **2016**, *50*, 13 6964.

[12] W. Wu, Y. Yang, H. Zhou, T. Ye, Z. Huang, R. Liu, Y. Kuang. *Water Air Soil Pollut.* **2012**, *224*, 1 1372.

[13] C. Su, R. Tandiana, J. Balapanuru, W. Tang, K. Pareek, C. T. Nai, T. Hayashi, K. P. Loh. *J. Am. Chem. Soc.* **2015**, *137*, 2 685.

[14] C. C. Caliman, A. F. Mesquita, D. F. Cipriano, J. C. C. Freitas, A. A. C. Cotta, W. A. A. Macedo, A. O. Porto. *RSC Adv.* **2018**, *8* 6136.

[15] K. Bustos-Ramirez, A. L. Martinez-Hernandez, G. Martinez-Barrera, M. d. Icaza, V. M. Castano, C. Velasco-Santos. *Materials* **2013**, *6*, 3 911.

[16] A. J. Paulista Neto, E. E. Fileti. *Phys. Chem. Chem. Phys.* **2018**, *20* 9507.

[17] J. Kim, L. J. Cote, F. Kim, W. Yuan, K. R. Shull, J. Huang. *Journal of the American Chemical Society* **2010**, *132*, 23 8180, pMID: 20527938.

[18] T. M. McCoy, G. Turpin, B. M. Teo, R. F. Tabor. *Curr. Opin. Colloid Interface Sci.* **2019**, *39* 98 .

[19] T. M. McCoy, M. J. Pottage, R. F. Tabor. *J. Phys. Chem. C* **2014**, *118*, 8 4529.

[20] S. Melle, M. Lask, G. G. Fuller. *Langmuir* **2005**, *21*, 6 2158.

[21] T. McCoy, S. Holt, A. Rozario, T. Bell, R. Tabor. *Adv. Mater. Interfaces* **2017**, *4*, 23 1700803.

[22] T. M. McCoy, H. C. Parks, R. F. Tabor. *Carbon* **2018**, *135* 164 .

[23] T. M. McCoy, A. C. Y. Liu, R. F. Tabor. *Nanoscale* **2016**, *8* 6969.

[24] J. Wang, F.-L. Hu, C. Li, J. Li, Y. Yang. *Sep. Purif. Technol.* **2010**, *73* 349.

[25] E. W. Hagan, M. N. Charalambides, C. R. Young, T. J. Learner, S. Hackney. *Prog. Org. Coat.* **2010**, *69*, 1 73 .

[26] D. Varade, P. Bahadur. *J. Surfact. Deterg.* **2004**, *7*, 3 257.

[27] J. Eastoe, M. H. Hatzopoulos, P. J. Dowding. *Soft Matter* **2011**, *7* 5917.

[28] W. Kunz, K. Holmberg, T. Zemb. *Curr. Opin. Colloid Interface Sci.* **2016**, *22* 99 .

[29] J. Aghion, S. B. Broyde, S. S. Brody. *Biochemistry* **1969**, *8* 3120.

[30] K. Stanton, C. Tibazarwa, H. Certa, W. Greggs, D. Hillebold, L. Jovanovich, D. Woltering, R. Sedlak. *Integr. Environ. Assess. Manag.* **2009**, *6* 155.

[31] Y. Cui, M. Threlfall, J. S. van Duijneveldt. *J. Colloid Interface Sci.* **2011**, *356*, 2 665 .

[32] H. Tan, W. Liu, D. Yu, H. Li, M. A. Hubbe, B. Gong, W. Zhang, H. Wang, G. Li. *Chem. Eng. Sci.* **2014**, *116* 682 .

[33] J. Berry, M. Neeson, R. Dagastine, D. Chan, R. Tabor. *J. Colloid Interface Sci.* **2015**, *454* 226.

[34] H. Vatanparast, A. Javadi, A. Bahramian. *Colloids Surf. A* **2017**, *521* 221.

[35] M. A. Creighton, Y. Ohata, J. Miyawaki, A. Bose, R. H. Hurt. *Langmuir* **2014**, *30*, 13 3687, pMID: 24625132.

[36] Y. Koga, F. Sebe, K. Nishikawa. *J. Phys. Chem. B* **2013**, *117*, 3 877.

[37] G. J. Silverberg, C. D. Vecitis. *Langmuir* **2017**, *33*, 38 9880, pMID: 28845996.

[38] P. Borthakur, P. K. Boruah, N. Hussain, B. Sharma, M. R. Das, S. Matić D. Řeha, B. Minofar. *J. Phys. Chem. C* **2016**, *120*, 26 14088.

[39] A. Nelson. *J. Appl. Crystallogr.* **2006**, *39*, 2 273.

[40] L. Pocivavsek, R. Dellsy, A. Kern, S. Johnson, B. Lin, K. Y. C. Lee, E. Cerda. *Science* **2008**, *320*, 5878 912.

[41] T. M. McCoy, L. de Campo, A. V. Sokolova, I. Grillo, E. I. Izgorodina, R. F. Tabor. *Phys. Chem. Chem. Phys.* **2018**, *20* 16801.